A Symbolic Representation Approach for the Diagnosis of Broken Rotor Bars in Induction Motors

Petros Karvelis, George Georgoulas, Ioannis P. Tsoumas, *Member, IEEE*, Jose Alfonso Antonino-Daviu, *Senior Member, IEEE*, Vicente Climente-Alarcón, *Member, IEEE*, and Chrysostomos D. Stylios, *Senior Member, IEEE*

***Abstract*—One of the most common deficiencies of currently existing induction motor fault diagnosis techniques is their lack of automatization. Many of them rely on the qualitative interpretation of the results, a fact that requires significant user expertise, and that makes their implementation in portable condition monitoring devices difficult. In this paper, we present an automated method for the detection of the number of broken bars of an induction motor. The method is based on the transient analysis of the start-up current using wavelet approximation signal that isolates a characteristic component that emerges once a rotor bar is broken. After the isolation of this component, a number of stages are applied that transform the continuous-valued signal into a discrete one. Subsequently, an intelligent icon-like approach is applied for condensing the relative information into a representation that can be easily manipulated by a nearest neighbor classifier. The approach is tested using simulation as well as experimental data, achieving high-classification accuracy.**

***Index Terms*—Discrete wavelet transform, intelligent icons, piecewise aggregate approximation (PAA), rotor faults, symbolic representation.**

NOMENCLATURE

f_{LSH}	Frequency of the left sideband harmonic (Hz).
s	Slip (–).
f_s	Power supply frequency (Hz).
f_{sampl}	Sampling frequency (Hz).
$x[\cdot]$	Discrete time signal (–).
$x(\cdot)$	Continuous time signal (–).
a_n	Approximation signal at level n (–).
d_j	Detail signal at level j (–).
a_i^n	Approximation coefficients at level n (–).
d_i^j	Detail coefficients at level j (–).
φ^n	Scaling function at level n (–).
ψ^j	Wavelet function at level j (–).
x_{PAA}	Piecewise aggregate approximation (PAA) representation of a signal/time series (–).
$\bar{x}[n]$	nth element of the PAA representation (–).
Σ	Alphabet.
$\lvert\Sigma\rvert$	Cardinality of the alphabet.

Manuscript received July 22, 2014; revised March 01, 2015 and June 11, 2015; accepted July 19, 2015. Date of publication August 02, 2015; date of current version October 02, 2015. This work was supported in part by the Spanish Ministerio de Economía y Competitividad (MINECO) and FEDER program in the framework of the Proyectos I+D del Subprograma de Generación de Conocimiento, Programa Estatal de Fomento de la Investigación Científica y Técnica de Excelencia (ref: DPI2014-52842-P). Paper no. TII-14-0766.

P. Karvelis, G. Georgoulas, and C. D. Stylios are with the Laboratory of Knowledge and Intelligent Computing, Department of Computer Engineering, Technological Educational Institute of Epirus, 47100 Artas, Greece (e-mail: pkarvelis@kic.teiep.gr; georgoul@kic.teiep.gr; stylios@teiep.gr).

I. P. Tsoumas is with the ABB Corporate Research, Baden-Dättwil 5405, Switzerland (e-mail: ytsoumas@ieee.org).

J. A. Antonino-Daviu is with the Instituto de Ingeniería Energética, Universitat Politècnica de València, 46022 Valencia, Spain (e-mail: joanda@die.upv.es).

V. Climente-Alarcón is with the Department of Electrical Engineering and Automation, Aalto University, 00076 Espoo, Finland (e-mail: viclial@ieee.org).

Color versions of one or more of the figures in this paper are available online at http://ieeexplore.ieee.org.

Digital Object Identifier 10.1109/TII.2015.2463680

I. INTRODUCTION

INDUCTION motors from a fraction of kilowatts up to several megawatts constitute the driving force of the industry [1]–[3]. Although they have lower efficiency and more volume and weight than permanent magnet synchronous motors, their low cost, simple construction, and robustness have led to their prevalence in industry applications, where the latter issues play a more crucial role. Furthermore, in such applications, the efficiency of the complete drive system including the working machine is more important than the efficiency of the motor; the improvement in the latter can only be marginal.

Regarding the low-voltage drives (400 V/690 V) with power ratings from several hundreds of kWs up to 1 MW, ca. 2/3 of the applications have to do with pumps, fans, and compressors [1]. The motors of the drive system in these applications are squirrel-cage induction motors with aluminum bars and rings for the rotor cage. No matter how robust the squirrel-cage motors are, they can still suffer from electrical and mechanical faults that can lead to failures and production shutdowns [4], [5]. Therefore, it is of paramount importance to detect a fault as precisely as possible and as early as possible; this will lead to a faster repair and a shorter downtime.

Motor current signature analysis (MCSA) is currently the most prominent approach for rotor fault diagnosis in asynchronous machines, [6]–[9], as well as to other electric equipments [10], primarily due to its noninvasive nature [11], [12].

It is known that a breakage of a bar in the rotor cage leads to a distortion in the air-gap magnetic field. More specifically, the effect of the breakage is typically represented by a “fault field” that is superposed to the normal field that is present under healthy conditions. The spatial waveform of the air-gap flux density caused by the fault field is a stepped bipolar wave, whose amplitude and spectral composition cyclically change over time. Rigorous characterization of this field can be found in [13]. This "fault field" induces multiple current harmonics in the stator windings. The identification of these harmonics in the Fourier spectrum of the steady-state current is the basis of the MCSA method [13]. In this regard, the evaluation of the amplitude of the left sideband harmonic (LSH) has drawn the most attention since this amplitude is closely related to the fault severity [2]. The frequency of the LSH is determined by the following equation [2], [14]:

$$f_{\mathrm{LSH}} = |1 - 2s| \cdot f_s \tag{1}$$

where f_s is the power supply frequency and s is the slip.

MCSA is predominantly used in many industrial sites as well as by most of the few available condition monitoring devices to assess the rotor condition [2]. Traditional MCSA has, however, important drawbacks as extensively reported by several authors [14], [15], such as the incorrect diagnostics of this tool (either false negatives or false positives) and its inability to cope with time-varying conditions, which can have huge economic repercussions [16], [17].

These problems of MCSA have justified the attempts to promote the industrial penetration of new advanced techniques. Indeed, some of them can avoid part of the MCSA constraints, increasing the reliability of the diagnostic procedure, as reported in several works. In this context, the analysis of the start-up current using advanced signal processing tools has been proven to be especially suitable; the fault-associated patterns appearing in the resulting time-frequency maps are very unlikely to be caused by a different phenomenon or reason, a fact that justifies its use, especially in controversial cases in which application of traditional MCSA is not suitable [16]–[18].

In spite of the advances in this area, most of these techniques still rely on a qualitative interpretation of the resulting patterns that must be carried out by an expert user [19]. In other words, the implementation of these techniques in unsupervised systems that do not require continuous human intervention is still in an experimental phase.

This work proposes a new, computationally efficient method to automate the detection process of rotor faults and produce an alarm in case of a detected fault. The proposed method is based on the transformation of the discrete time, continuous-valued wavelet approximation signal [13] of the start-up current, to a discrete time, discrete-valued signal. The process known as discretization or symbolization allows for the application of highly efficient algorithms successfully applied at other fields such as bioinformatics or text mining [20], which may come handy in embedded system implementation or online monitoring. Moreover, symbolic data representation is usually less sensitive to measurement noise, a situation which often occurs in industrial environments [21].

In the field of electric equipment condition monitoring, symbolic representations have been primarily used for anomaly detection [22] using statistical properties of the generated symbolic sequences. Symbolic dynamics were involved in the detection of broken bars both for inverter-fed [23] and line-fed motors [24], and for the detection of stator voltage imbalance in induction motors [25]. In [26], a variety of fault conditions in an induction motor (voltage imbalance, bearing faults, broken bars) were detected using symbolic filtering. In [27], the demagnetization of permanent magnet machines was estimated, while in [28] the state of charge of a battery was estimated using symbolic time series analysis.

All the aforementioned symbolic dynamic approaches involve steady-state operation. In [29], the Symbolic Aggregate approXimation (SAX) method was employed for the detection of broken bars during start-up. An intelligent icons [30] representation capable of discriminating between healthy and faulty situations is presented [29] without however being able to quantify the severity of the fault. In [31], the information extracted from the second complex intrinsic mode function (IMF) of the start-up current was condensed into a symbolic time series which was then classified using a scheme based on discrete hidden Markov models (HMMs).

In this work, an approach that builds upon the basic blocks of SAX but uses a different partitioning for the discretization process is proposed. The achieved results using both simulated and experimental data are promising, indicating the potential use of the method for the automatic identification of broken bars in induction motors.

This paper is structured as follows. Section II provides the necessary background of the different components of the proposed procedure along with the description of the method. Section III presents the testing procedure and the achieved results both for the simulation and the experimental test case. Finally, Section IV concludes the paper providing also some hints for future work.

II. Proposed Procedure

The proposed diagnostic procedure is depicted in Fig. 1, and as it can be seen, it involves a number of stages. In the rest of the section, the technical background of each of the stages is presented.

A. Discrete Wavelet Transform for the Extraction of the Fault-Related Approximation Signal

Discrete wavelet transform (DWT) decomposes a signal $x(t)$ into an approximation signal and a number of detail signals, each one representing a particular "coarseness" of the signal

$$\begin{aligned} x(t) &= \sum_i a_i^n \varphi_i^n(t) + \sum_i \sum_j^n d_i^j \psi_i^j(t) \\ &= a_n + \sum_{j=1}^n d_j \end{aligned} \tag{2}$$

where a_n and d_j are the approximation signal at level n and the detail signal at level j, respectively, which in turn are constructed by the scaling a_i^n and wavelet coefficients d_i^j using the scaling φ^n and wavelet functions ψ^j.

Signals containing a mixture of features that reside at different time and frequency resolutions are well-suited for DWT analysis [32]. The detail signal $d_j(t)$ represents the frequency

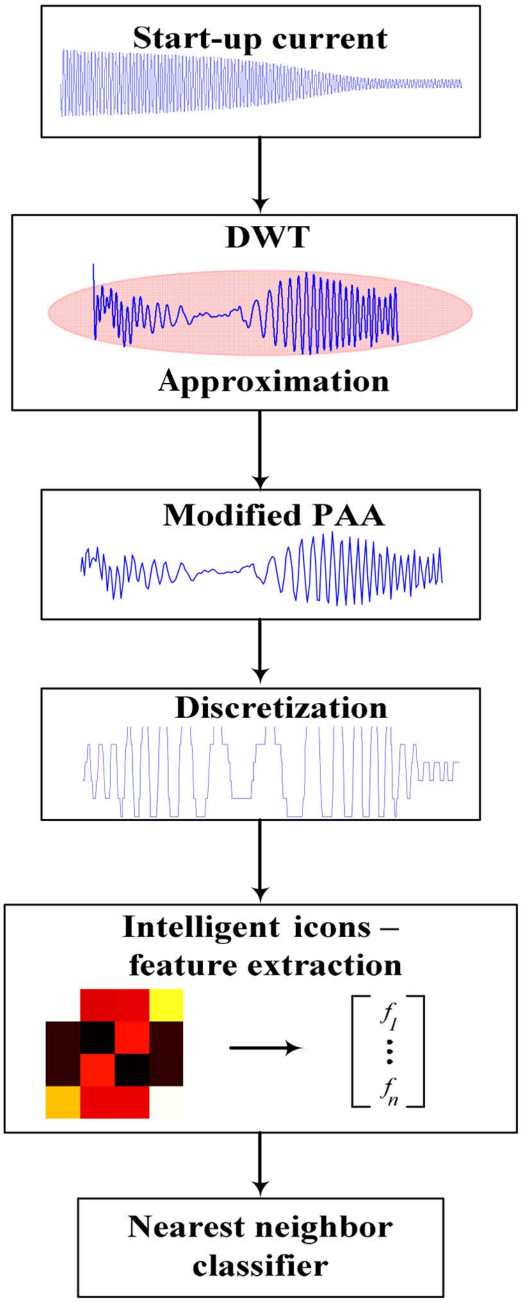

Fig. 1. Proposed diagnostic approach.

content of the signal $x(t)$ residing in $\left[f_{\text{samp}}/2^{j+1}, f_{\text{samp}}/2^{j}\right]$, where f_{samp} is the sampling frequency. The lowest frequency content $\left[0, f_{\text{samp}}/2^{n+1}\right]$ of the original signal $x(t)$ is represented by the approximation signal $a_n(t)$.

As it has been shown in [13], [16], [18], and [33], in the case of broken rotor bars, the faulty component can be "isolated" by the approximation signal $a_n(t)$, provided that a suitable decomposition level is selected. For example, for the case of $f_{\text{samp}} = 5$ kHz and $f_s = 50$ Hz, the appropriate level is 6, with the approximation signal containing frequencies $[0, 39.06]$ Hz [18]. This specific interval has been proven quite effective in isolating the evolution of the LSH [18] (even though more

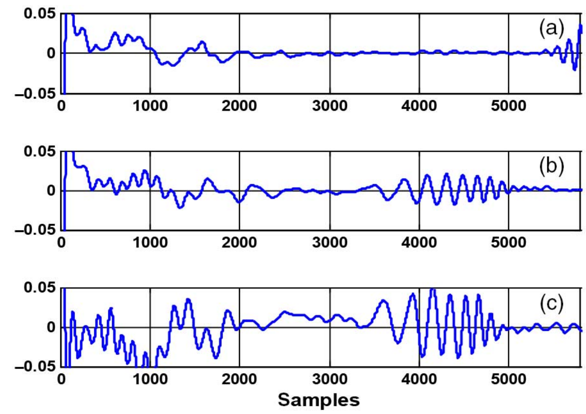

Fig. 2. Approximation signal of the start-up current for (a) a healthy machine, (b) a machine with one broken bar, and (c) a machine with two broken bars under no load condition.

elaborate uses of the DWT have been proposed [34]). When a different f_{samp} is used that does not lead to that specific frequency content, sampling rate conversion can be achieved using polyphase filters [35].

Different mother wavelets have been used for the extraction of the approximation signal [13], [18], with satisfactory results. In this work, the dmeyer (discrete Meyer wavelet) is selected and used in all conducted experiments [18]. In Fig. 2, the approximation signal at level 6 (which corresponds to the $[0, 39.06]$ Hz interval—5 kHz sampling frequency) of the start-up current of the laboratory motor described in the Appendix (Table IV) is depicted at no load condition for a healthy, a one broken bar and a two broken bar situation. Note that all currents are normalized to have maximum amplitude approximately equal to one before the application of the DWT.

B. Piecewise Aggregate Approximation

PAA, which was independently proposed in [36] and [37], divides a discrete time signal (a time series) $x = \{x[1], x[2], \ldots, x[N]\}$ of length N, into w segments of equal length (N/w) and then each segment is replaced by the average value of the segment, creating a new time series $x_{\text{PAA}} = \{\bar{x}[1], \bar{x}[2], \ldots, \bar{x}[w]\}$ where

$$\bar{x}[i] = \frac{w}{N} \sum_{j=\frac{N}{w}(i-1)+1}^{\frac{N}{w}i} x[j], \quad \text{for } i = 1, 2, \ldots, w. \qquad (3)$$

An example of the PAA representation of a time series is shown in Fig. 3. PAA is used as an effective first stage of dimensionality reduction increasing computational efficiency.

PAA assumes that N can be divided exactly by w. A modified version that can handle situations where N cannot be divided exactly by w was proposed as part of the generalized SAX [38], [39]. Assuming that the discrete time signal has a normalized sampling period ($x = \{x[nT]\}, n = 1, 2, \ldots, N$ and $T = 1$), an analytic expression for the calculation of

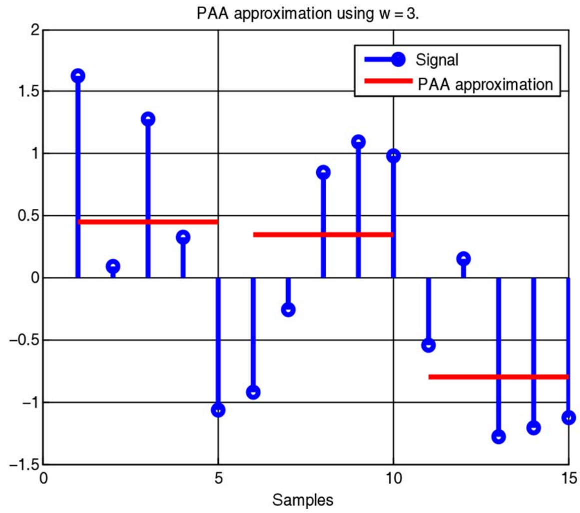

Fig. 3. Example of the application of PAA to a signal with only 15 samples (marked with open circles) using $w = 3$. Each consecutive nonoverlapping five-sample long segment is averaged to produce the PAA representation.

generalized PAA can be written in a summation form as follows [40]:

$$\begin{aligned}\bar{x}[i] = {}& \frac{w}{N}\left(\left(\left(\frac{N}{w}i+1\right) - \left\lfloor \frac{N}{w}i+1\right\rfloor\right)\cdot x\left[\left\lfloor \frac{N}{w}i+1\right\rfloor\right]\right)\\ &+ \frac{w}{N}\left(\sum_{j=\left\lfloor \frac{N}{w}(i-1)+1\right\rfloor+1}^{\left\lfloor \frac{N}{w}i+1\right\rfloor-1} x[j]\right)\\ &+ \frac{w}{N}\left(\left(1-\left(\left(\frac{N}{w}(i-1)+1\right)-\left\lfloor\frac{N}{w}(i-1)+1\right\rfloor\right)\right)\right.\\ &\left.\cdot\, x\left[\left\lfloor \frac{N}{w}(i-1)+1\right\rfloor\right]\right) \qquad \text{for } i=1,2,\ldots,w \end{aligned} \tag{4}$$

where $\lfloor y \rfloor$ is the greatest integer less than or equal to y. Equation (4) reduces to (3) when N can be divided exactly by w.

C. Discretization

The discretization of a continuous-valued signal for the creation of a sequence of symbols drawn from an alphabet Σ is performed by partitioning the range of the input signal into a number of disjoint regions. In this work, the maximum entropy partitioning (MEP) is adopted [41]. As its name implies, MEP creates symbols in such a way as to maximize the entropy of the created string. For a discrete time continuous-valued signal with w samples and for an alphabet with cardinality $|\Sigma|$, the MEP procedure is as follows [41], [42].

1) Sort the samples of the original discrete time continuous-valued signal in an ascending order.
2) Define the partitioning limits starting from the first point of the sorted signal from the first step such as $\lfloor w/|\Sigma| \rfloor$ data points will lie within each section.
3) Use the partition obtained in the second step, to transform the original discrete time continuous-valued signal to a string of symbols (if the value of a data point lies within or on the lower bound of a partition, it is coded with the symbol associated with that partition).

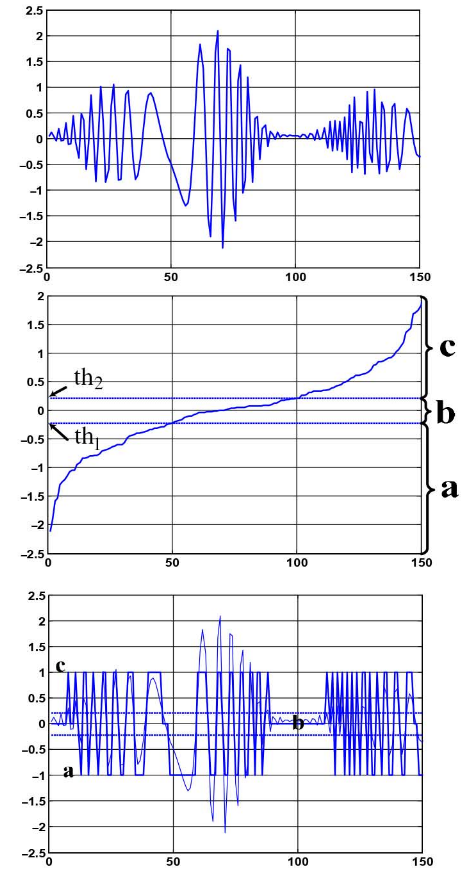

Fig. 4. Schematic explanation of the sequence creation process for the case of a three-symbol alphabet. The original signal is shown on the top of the figure. In the middle, the partitioning using the MEP is depicted, with the thresholds dividing the samples into three regions, with each one containing 50 samples, leading to three equiprobable symbols. The bottom caption shows the transformation of the original signal into a sequence. For illustrative purposes, we only depict the sequence as a continuous plot overlaid on the original signal, which is depicted in the background using a dashed line.

A graphical representation of the procedure is depicted in Fig. 4 for the case of an alphabet with only 3 symbols (“a,” “b,” “c”) and 150 samples (the value of the 50th sample of the sorted series defines the lower cutting point (th_1) while the value of the 100th sample defines the upper cutting point (th_2)—therefore, any sample which has a value lower or equal than th_1 will be assigned the symbol “a,” any sample which has a value that is higher than th_1 and lower or equal than th_2 will be assigned the symbol “b” and the rest of the samples will be assigned the symbol “c”). As it can be seen with that partition all three symbols are equipropable (“a,” “b,” and “c” appear 50 times each), therefore leading to a maximization of the entropy.

MEP allows for more symbols—finer resolution—in regions with higher information content, while regions with lower information content undergo a sparser partitioning with fewer symbols assigned.

D. Feature Extraction—Intelligent Icons

All the previous steps have led to the creation of a symbolic sequence. This sequence is further condensed in order to come up with a probabilistic representation. Along these lines the simplest approach is to use the intelligent icons [30], [43]

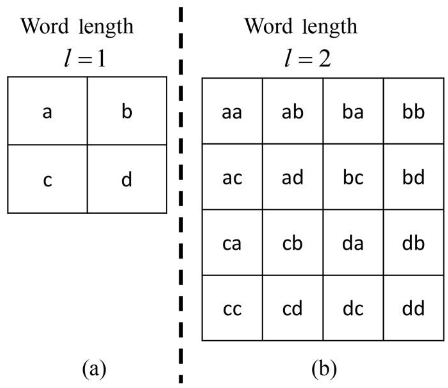

Fig. 5. Two mappings for two different word lengths, (a) $l = 1$ and (b) $l = 2$ for an alphabet $\Sigma = \{a, b, c, d\}$ of size $|\Sigma| = 4$.

method with or without the illustration part. The idea behind the intelligent icons is to count the occurrences of symbols or words of symbols creating this way, approximations of the underlying probability mass functions. The rational is similar to the D-Markov modeling approach employed in [24]–[26], where a transition matrix is created by counting transitions between states (where each state is just a word of length D).

For creating an intelligent icon first, we assign to each letter of the alphabet a unique value k

$$a = 0,\ b = 1,\ c = 2,\ d = 3. \tag{5}$$

Each word has an index for the location of each symbol in the table of the icon. For clarity, we can show them explicitly as subscripts. For example, if the first word is $\alpha_0\alpha_1$ then $k_0 = a = 0$ and $k_1 = a = 0$. In order to map a subword to the table represented by the icon, we can use a mapping like the ones presented in Fig. 5.

The following equations can be used in order to find the row and column of each subword in the intelligent icon table:

$$\text{col} = \sum_{n=0}^{l-1} (k_n \cdot 2^{l-n-1}) \bmod 2^{l-n} \tag{6}$$

$$\text{row} = \sum_{n=0}^{l-1} (k_n \text{div} 2) \cdot 2^{l-n-1} \tag{7}$$

where mod represents the modulo operation and div the integer division operation.

For example, for the subword aa, where $k_0 = a = 0$, $k_1 = a = 0$, and $l = 2$; substituting in (6) and (7), we get col $= 1$ and row $= 1$, respectively [the first element of the mapping of Fig. 5(b)].

Intelligent Icons, also called intelligent bitmaps [43], were originally developed to display time series in a more compact form. Along this line, Fig. 6 displays the intelligent icons for the case of a healthy machine and a machine with one and two broken bars, which is described in Section III-B, for different durations of the start-up phenomenon. As it can be seen the icons are pretty distinct.

However, in this work, the goal is not to trade one representation [one-dimensional (1-D) time series] for another (a 2-D icon) rather than to develop an automated procedure for the

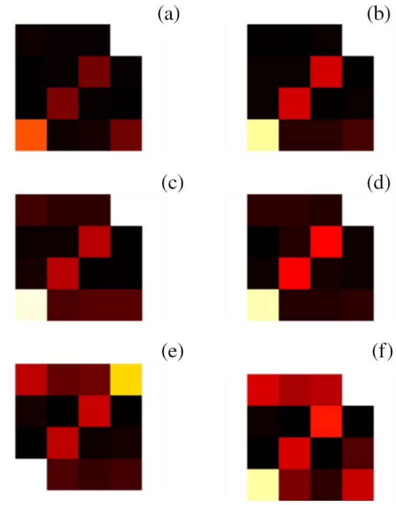

Fig. 6. Intelligent Icons representation of the approximation signal using, $w = 250$, $|\Sigma| = 4$, and word length equal to 2 for the case of a normal machine (a) and (b), a machine with one broken bar (c)–(d), and a machine with two broken bars (e)–(f). The start-up signals come from an actual machine (Section III-B). Icons (a), (c), and (e) correspond to no load and (b), (d), and (f) to half-load condition.

diagnosis of broken bars. Therefore, the estimated probability mass functions of the words are treated as feature vectors to be fed into a classifier. This is a similar to the bag-of-patterns representation proposed in [44], which was inspired by the bag-of-words representation from information retrieval and text mining.

E. Classification-Diagnosis

The final stage of the proposed approach consists of the nearest neighbor (NN) classifier, the simplest member of the k-NN family [46]. This, as its name implies, given a labeled training set, assigns a new unseen example to the class of its NN, where the “closeness” is assessed through an appropriately selected distance.

The NN classifier has the desired property [47] of being a parameter-free algorithm, leaving the tuning process entirely to the selection of the parameters involved during the application of PAA, the discretization and the selection of the word length as it will be explained in the next section.

III. Experimental Procedure—Results

The proposed method was tested using both simulation data and data coming from a squirrel cage induction machine and three large industrial motors. The evaluation procedure involved, as well as the achieved results, is presented in the rest of this section.

A. Simulation Results

Simulated signals were obtained using a model derived from an analytical model of induction machine under fault that was developed in MATLAB Simulink environment. The model is able to simulate induction machines with rotor asymmetries

TABLE I
CLASSIFICATION ACCURACY

	Healthy (%)	One broken bar (%)	Two broken bars (%)	Overall
Simulation	100	100	100	100
*ExperimentalA1	100	100	100	100
**ExperimentalA2	100	100	100	100
***ExperimentalA3	100	100	100	100
+ExperimentalB1	100	100	90	96.7
++ExperimentalB2	100	100	100	100
+++ExperimentalB3	100	100	100	100

*ExperimentalA1: full load data for testing.
**ExperimentalA2: no load data for testing.
***ExperimentalA3: half load data for testing.
+ExperimentalB1: no load data for training.
++ExperimentalB2: half load data for training.
+++ExperimentalB3: full load data for training.

and eccentricity in different load conditions, both stationary and transient states and yielding magnitudes such as currents, speed, and torque [48].

Ten healthy start-ups and ten start-ups for each one of the faulty conditions (one and two broken bars) were simulated with different durations of the transient phenomenon. Therefore, a total of 30 cases were considered each one of them being different from all the rest.

To assess the performance of the approach a 10-fold (stratified) cross-validation (CV) procedure was repeated 10 times (outer loop) (10×10 CV) [49]. This means that each time 3 cases (one from each condition) were left out and the rest 27 cases ($9 + 9 + 9$) were used for training, and the whole procedure was repeated 10 times with reshuffling taking place between the 10 different runs of the outer loop. This way, the training and testing sets are not the same in any of the 10 different runs/repetitions. This procedure is adopted in order to avoid overoptimistic or overpessimistic results due to a particular partition of the data. Moreover, for the tuning of the algorithm, i.e., for selecting the number of windows w (250, 500, 1000, or 2000), the alphabet size $|\Sigma|$ (4, 5, 6, 7, or 8) as well as the word length (2 or 3), a nested procedure involving a grid search was performed using only the training data at each fold. This way the estimation of the performance was decoupled from the tuning process [49]. During the training process, the MEP approach operated on the pooled sample of all the training signals. This way the different amplitude of the chirp-like components in the case of the one and the two broken bars were taken into account. Moreover, since the beginning and the ending of the recordings are similar for almost all cases, 20% of the recorded signal was excluded from further processing.

The classification results for the simulation data are depicted at the first row in Table I indicating perfect discrimination performance of the proposed approach.

B. Experimental Results—Laboratory Machine Under Different Loading Conditions

For the first part of experimental evaluation, the squirrel cage induction motor of the Appendix (Table IV) was coupled directly to a DC machine (load). Healthy and faulty rotors (with one and two broken bars artificially forced by drilling a hole in the corresponding bar, just in the junction point between the bar and the short-circuit end ring) were tested. A picture of one of the rotors (with one broken bar) is depicted in Fig. 7.

Fig. 7. Picture of the rotor with one broken bar.

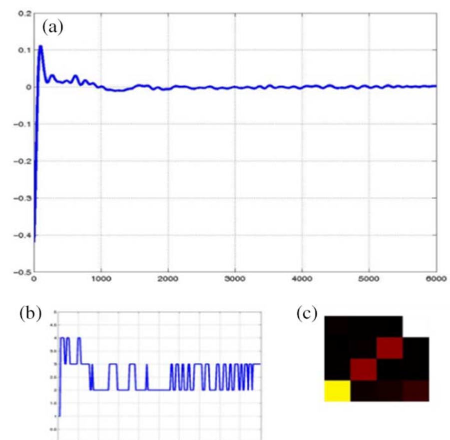

Fig. 8. Illustration of the main stages of the proposed procedure for a healthy machine operating at half load. (a) Approximation signal. (b) Discrete representation. (c) Intelligent icon representation.

This first set of experiments aims to test the variability of the approach under different loading conditions. More specifically, a number of start-up signals were acquired under different loading conditions with different durations of the transient phenomenon. Figs. 8–10 depict the approximation signal, its discrete representation as well the illustration of the extracted features in the form of an intelligent icon for three different cases (healthy–one broken bar–two broken bars) at half load condition ($|\Sigma| = 4$, $w = 500$, and word length equal to 2) for the machine described in the Appendix (Table IV). Stator currents throughout the experimental evaluation were sampled with a frequency of 5 kHz. Therefore, the approximation signal was acquired using DWT up to level 6. The experimental data collected is summarized in Table II.

This experimental setting involved the use of data coming from two loading conditions for training and the third one for testing (i.e., no-load and half load for training and full load for testing). Therefore, three sets of experiments were carried out. For the selection of the parameters, an internal CV procedure was carried out within the training set.

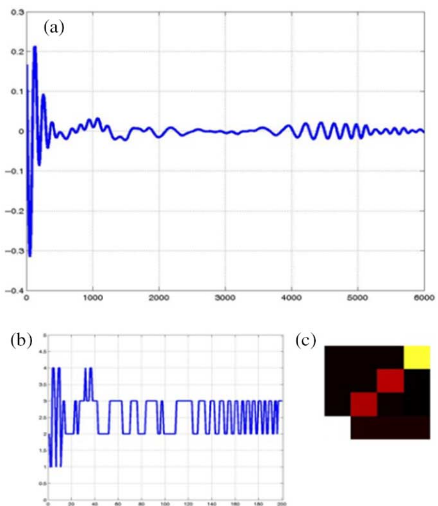

Fig. 9. Illustration of the main stages of the proposed procedure for a machine with one broken bar operating at half load. (a) Approximation signal. (b) Discrete representation. (c) Intelligent icon representation.

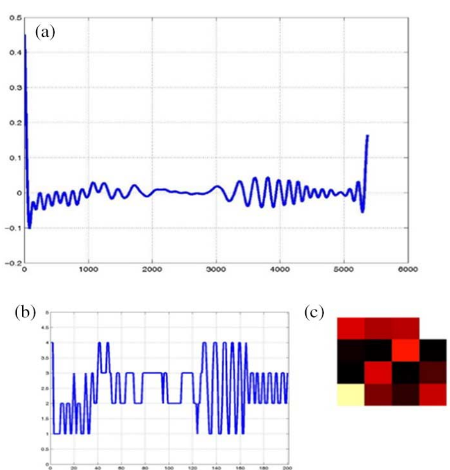

Fig. 10. Illustration of the main stages of the proposed procedure for a machine with two broken bars operating at half load. (a) Approximation signal. (b) Discrete representation. (c) Intelligent icon representation.

TABLE II
EXPERIMENTAL DATA FOR THE LABORATORY MOTOR

	Healthy	One broken bar	Two broken bars
No load	5	5	5
Half load	5	5	5
Full load	5	5	5

The same procedures as in the case of the simulation study (pooling together of the training data for the determination of the breaking points, exclusion of the first and last 20% samples of the approximation) were employed and the results are summarized in Table I (rows 2–4). As it can be seen, the method seems to be robust to load variations, capable to "extrapolate" to unseen situations.

To further test the approach, a second set of experiments was carried out. This time data from only one loading condition were involved for training and the data from the other two conditions were reserved for testing. In effect, the training and testing data sets of the previous experimental study were switched. The same training protocol was employed. The results are also summarized in Table I (rows 5–7). As it can be seen in almost all cases but one data from a single condition can be used effectively for building a diagnostic module. Only in the case of a model trained using only data coming from no load conditions, the method mistakenly assigned a case of two broken bars to the class of one broken bar (therefore, 9/10 of the two broken bar cases were correctly classified and in total 29/30 of all involved test cases).

TABLE III
ASSESSMENT OF THE LARGE MOTORS

Motor label	Condition
M1	Two broken bars
M2	One broken bar
M3	Healthy

C. *Experimental Results—Industrial Large Machines*

In the previous section, we examined the efficiency of the method to diagnose the condition of an induction machine operating at different loading conditions. To corroborate the validity of the methodology in other machines and, hence, to prove its ability to generalize, several real field motor signals were used. All motors were operating in real mining facilities and the start-up current signals were obtained during one of the periodic inspections of these machines. The general characteristics of the field motors are provided in the Appendix (Tables V–VII). Note that these are very large motors that substantially differ from the motor tested in the laboratory.

Two of the field motors (M1 and M2) had different levels of rotor asymmetry. In the case of motor M1, the rotor asymmetry was confirmed after rotor disassembly and visual inspection, while in the case of M2, there were clear symptoms of rotor asymmetry. On the other hand, motor M3 was a healthy machine.

For this experiment, the data collected from the laboratory motor (Table II) were used to train the classifier. The assessment of the three motors based on the proposed method is summarized in Table III. We must note that sampling rate conversion took place since for M1 the sampling rate was 6 kHz, while for M2, the sampling rate was 4048 Hz and all the training signals were sampled at 5 kHz.

The trained classifier was able to detect that motors M1 and M2 had asymmetries without signaling a false alarm for M3. The results are consistent with the fact that the method assigned to M1 the class with the higher rotor asymmetry trained to recognize (two broken bars), while assigning M2 to the category of one broken bar.

IV. CONCLUSION

An automated method for the diagnosis of broken bars using the information contained in the start-up current was presented, which can be used to signal an alarm for further inspection.

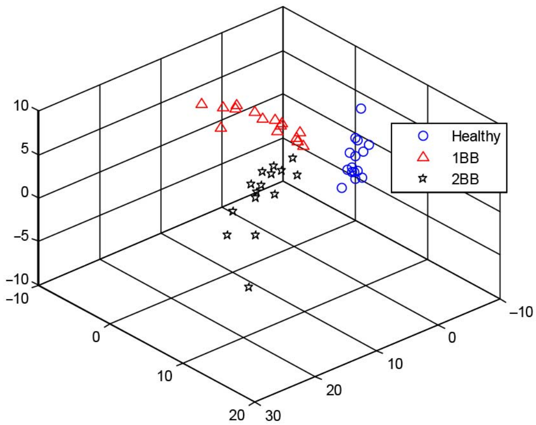

Fig. 11. Projection of the data coming from the laboratory setting into three dimensions, using, $w = 2000$, $|\Sigma| = 8$, and word length equal to 2. The circles correspond to the healthy condition, the triangles to one broken bar and stars to two broken bars.

The method combines DWT for the isolation of a faulty component that arises in the case of a bar brakeage, and a symbolic analysis approach for transforming the information contained in the component isolated in the previous stage to useful information. The efficiency of the method was tested using both simulated and experimental data and a very simple classifier proving that once the feature engineering step is suitable [47] simple methods can be used for the final classification stage. As in most data-driven methods, the more representative data available during the training period, the better. This was verified during the different experiments involving the laboratory data where the only misclassification occurred when a reduced set of data (only one loading condition) was used for training. However, even in that case, the method did not confuse healthy with faulty conditions.

The efficiency of the representation can be highlighted by inspecting Fig. 11, which depicts the projection of the data coming from the laboratory setting into three dimensions using classic multidimensional scaling. As it can be seen, even in this low-dimensional space where the discrimination might be a bit compromised the three classes/conditions seem to occupy different portions of the space even though the one and two broken bar categories can be quite close at some parts of that space. This is probably the reason for the one misclassification that occurred during the "ExperimentalB1" set up. On the other hand, the healthy class seems to be quite distinct from the faulty ones.

Compared to [29], this method is not only capable of detecting the presence of fault but it can also discriminate between one and two broken bars. Furthermore, the method is very simple and the whole process requires minimum intervention, contrary to the method proposed in [31], where all three currents should be monitored, while the discretization was based on expert judgement and the classifier was much more complex than the simple one used in this study.

Moreover, the method was tested using also real-life data. Even though no additional data were available for motor M1–M3, the method was capable to discriminate the healthy motor M3 from the two faulty motors. The promising results indicate that the approach can be used at least in an anomaly detection scenario. Nevertheless, further testing is needed before its adoption into industrial practice, along with testing with the simultaneous presence of other common faults.

Furthermore, the method was tested only for completely broken bars. In future work, more demanding scenarios will be pursued with only partially broken bars and under accelerated testing conditions to investigate the potential of the proposed approach to be integrated in a prognostic framework.

In addition to this, in future work, the diagnostic problem will also be tested in the more demanding inverter-fed scenario as well as under the use of fault tolerant controllers, which might attenuate the fault signature.

Appendix

Rated characteristics of the tested motors.

TABLE IV
Laboratory Motor

Rated power	1.1 kw
Rated frequency	50 Hz
Rated voltage	400 V
Rated primary current	2.7 A
Rated speed	1410 rpm
Rated slip	0.06
Connection	Star
Number of pole pairs	2
Number of rotor bars	28
Number of stator slots	36

TABLE V
Field Motor: M1

Application	High speed coal mill
Rated power	320 kW
Rated frequency	50 Hz
Rated speed	740 rpm
Number of poles	8

TABLE VI
Field Motor: M2

Application	Mill fan
Rated power	400 kW
Rated frequency	50 Hz
Rated speed	1492 rpm
Number of poles	4

TABLE VII
Field Motor: M3

Application	Compressor
Rated power	1.2 MW
Rated frequency	50 Hz
Rated speed	2998 rpm
Number of poles	2 poles

REFERENCES

[1] D. B. Durocher and G. R. Feldmeier, "Predictive versus preventive maintenance," *IEEE Trans. Ind. Appl.*, vol. 10, no. 5, pp. 12–21, Oct. 2004.

[2] W. T. Thomson and M. Fenger, "Current signature analysis to detect induction motor faults," *IEEE Ind. Appl. Mag.*, vol. 7, no. 4, pp. 26–34, Jul./Aug. 2001.

[3] V. Sousa Santos, P. R. V. Felipe, J. R. Gomez Sarduy, N. Lemozy, A. Jurado, and E. C. Quispe, "Procedure for determining induction motor efficiency working under distorted grid voltages," *IEEE Trans. Energy Convers.*, vol. 30, no. 1, pp. 331–339, Mar. 2015.

[4] Allianz Insurance, Germany (1996-1999), "Allianz survey," VDE Colloquium, Berlin, Germany, Jun. 28, 2001.

[5] P. Zhang, Y. Du, T. G. Habetler, and B. Lu, "A survey of condition monitoring and protection methods for medium-voltage induction motors," *IEEE Trans. Ind. Appl.*, vol. 47, no. 1, pp. 34–46, Jan./Feb. 2011.

[6] M. Riera-Guasp, J. A. Antonino-Daviu, and G. A. Capolino, "Advances in electrical machine, power electronic and drive condition monitoring and fault detection: State of the art," *IEEE Trans. Ind. Electron.*, vol. 62, no. 3, pp. 1746–1759, Mar. 2015.

[7] M. Sahrauoi, A. J. M. Cardoso, and A. Ghoggal, "The use of modified Prony method to track the broken rotor bar characteristic frequencies and amplitudes in three-phase induction motors," *IEEE Trans. Ind. Appl.*, vol. 51, no. 3, pp. 2136–2147, May/Jun. 2015.

[8] S. H. Kia, H. Henao, and G.-A. Capolino, "Efficient digital signal processing techniques for induction machine fault diagnosis," in *Proc. IEEE Workshop Elect. Mach. Des. Control Diagnosis (WEMDCD)*, Paris, France, 2013, pp. 233–246.

[9] K. N. Gyftakis and J. C. Kappatou, "The zero-sequence current as a generalized diagnostic mean in Δ-connected three-phase induction motors," *IEEE Trans. Energy Convers.*, vol. 29, no. 1, pp. 138–148, Mar. 2014.

[10] B. M. Ebrahimi, M. J. Roshtkhari, J. Faiz, and S. V. Khatami, "Advanced eccentricity fault recognition in permanent magnet synchronous motors using stator current signature analysis," *IEEE Trans. Ind. Electron.*, vol. 61, no. 4, pp. 2041–2052, Apr. 2014.

[11] M. B. K. Bouzid and G. Champenois, "New expressions of symmetrical components of the induction motor under stator faults," *IEEE Trans. Ind. Electron.*, vol. 60, no. 9, pp. 4093–4102, Sep. 2013.

[12] M. J. Picazo-Rodenas, J. Antonino-Daviu, V. Climente-Alarcon, R. Royo-Pastor, and A. Mota-Villar, "Combination of non-invasive approaches for general assessment of induction motors," *IEEE Trans. Ind. Appl.*, vol. 51, no. 3, pp. 2172–2180, May/Jun. 2015.

[13] M. Riera-Guasp, J. A. Antonino-Daviu, J. Roger-Folch, and M. P. Molina Palomares, "The use of the wavelet approximation signal as a tool for the diagnosis of rotor bar failures," *IEEE Trans. Ind. Appl.*, vol. 44, no. 3, pp. 716–726, May/Jun. 2008.

[14] F. Filippetti, A. Bellini, and G. Capolino, "Condition monitoring and diagnosis of rotor faults in induction machines: State of art and future perspectives," in *Proc. IEEE Workshop Elect. Mach. Des. Control Diagnosis (WEMDCD)*, 2013, pp. 196–209.

[15] G. M. Joksimovic, J. Riger, T. M. Wolbank, N. Peric, and M. Vasak, "Stator-current spectrum signature of healthy cage rotor induction machines," *IEEE Trans. Ind. Electron.*, vol. 60, no. 9, pp. 4025–4033, Sep. 2013.

[16] J. A. Antonino-Daviu, M. Riera-Guasp, J. R. Folch, and M. Pilar Molina Palomares, "Validation of a new method for the diagnosis of rotor bar failures via wavelet transform in industrial induction machines," *IEEE Trans. Ind. Appl.*, vol. 42, no. 4, pp. 990–996, Jul./Aug. 2006.

[17] J. Park *et al.*, "Evaluation of the detectability of broken rotor bars for double squirrel cage rotor induction motors," in *Proc. IEEE Energy Convers. Congr. Expo. (ECCE)*, Sep. 2010, pp. 2493–2500.

[18] M. Riera-Guasp, J. A. Antonino-Daviu, M. Pineda-Sanchez, R. Puche-Panadero, and J. Perez-Cruz, "A general approach for the transient detection of slip-dependent fault components based on the discrete wavelet transform," *IEEE Trans. Ind. Electron.*, vol. 55, no. 12, pp. 4167–4180, Dec. 2008.

[19] E. Cabal-Yepez, A. G. Garcia-Ramirez, R. J. Romero-Troncoso, A. Garcia-Perez, and R. A. Osornio-Rios, "Reconfigurable monitoring system for time-frequency analysis on industrial equipment through STFT and DWT," *IEEE Trans. Ind. Informat.*, vol. 9, no. 2, pp. 760–771, May 2013.

[20] J. Lin, E. Keogh, S. Lonardi, and B. Chiu, "A symbolic representation of time series, with implications for streaming algorithm," in *Proc. 8th ACM SIGMOD Workshop Res. Issues Data Mining Knowl. Discovery*, San Diego, CA, USA, 2003, pp. 2–11.

[21] C. S. Daw, C. E. A. Finney, and E. R. Tracy, "A review of symbolic analysis of experimental data," *Rev. Sci. Instrum.*, vol. 74, no. 2, pp. 915–930, 2003.

[22] A. Ray, "Symbolic dynamic analysis of complex systems for anomaly detection," *Signal Process.*, vol. 84, no. 7, pp. 1115–1130, 2004.

[23] R. Samsi, V. Rajagopalan, and A. Ray, "Wavelet-based symbolic analysis for detection of broken rotor bars in inverter-fed induction motors," in *Proc. IEEE Amer. Control Conf.*, 2006, pp. 3032–3037.

[24] R. Samsi, V. Rajagopalan, and A. Ray, "Wavelet-based symbolic analysis for detection of broken rotor bars in inverter-fed induction motors," in *Proc. IEEE Amer. Control Conf.*, 2006, pp. 3032–3038.

[25] R. Samsi, A. Ray, and J. Mayer, "Early detection of stator voltage imbalance in three-phase induction motors," *Elect. Power Syst. Res.*, vol. 79, no. 1, pp. 239–245, 2009.

[26] R. A. Gupta, A. K. Wadhwani, and S. R. Kapoor, "Early estimation of faults in induction motors using symbolic dynamic-based analysis of stator current samples," *IEEE Trans. Energy Convers.*, vol. 26, no. 1, pp. 102–114, Mar. 2011.

[27] S. Chakraborty, E. Keller, A. Ray, and I. Mayer, "Detection and estimation of demagnetization faults in permanent magnet synchronous motors," *Elect. Power Syst. Res.*, vol. 96, pp. 225–236, 2013.

[28] Y. Li, P. Chattopadhyay, and A. Ray, "Dynamic data-driven identification of battery state-of-charge via symbolic analysis of input–output pairs," *Appl. Energy*, vol. 155, pp. 778–790, 2015.

[29] P. Karvelis, I. P. Tsoumas, G. Georgoulas, C. D. Stylios, J. A. Antonino-Daviu, and V. Climente-Alarcon, "An intelligent icons approach for rotor bar fault detection," in *Proc. Annu. Conf. IEEE Ind. Electron. Soc. (IECON'13)*, 2013, pp. 5526–5531.

[30] E. Keogh, L. Wei, X. Xi, S. Lonardi, J. Shieh, and S. Sirowy, "Intelligent icons: Integrating lite-weight data mining and visualization into GUI operating systems," in *Proc. 6th Int. Conf. Data Mining (ICDM'06)*, 2006, pp. 912–916.

[31] G. Georgoulas *et al.*, "Automatic pattern identification based on the complex empirical mode decomposition of the startup current for the diagnosis of rotor asymmetries in asynchronous machines," *IEEE Trans. Ind. Electron.*, vol. 61, vo. 9, pp. 4937–4946, Sep. 2014.

[32] S. Mallat, *A Wavelet Tour of Signal Processing*, 2nd ed. New York, NY, USA: Academic, 1999.

[33] J. Antonino-Daviu, M. Riera-Guasp, M. Pineda-Sanchez, and R. Pérez, "A critical comparison between DWT and Hilbert–Huang-based methods for the diagnosis of rotor bar failures in induction machines," *IEEE Trans. Ind. Appl.*, vol. 45, no. 5, pp. 1794–1803, Sep./Oct. 2009.

[34] J. Antonino-Daviu, S. Aviyente, E. G. Strangas, and M. Riera-Guasp, "Scale invariant feature extraction algorithm for the automatic diagnosis of rotor asymmetries in induction motors," *IEEE Trans. Ind. Informat.*, vol. 9, no. 1, pp. 100–108, Feb. 2013.

[35] J. G. Proakis and D. G. Manolakis, *Digital Signal Processing: Principles, Algorithms, and Applications*, 4th ed. Englewood Cliffs, NJ, USA: Prentice-Hall, 2007.

[36] E. Keogh, K. Chakrabarti, M. Pazzani, and S. Mehrotra, "Dimensionality reduction for fast similarity search in large time series databases," *J. Knowledge Inf. Syst.*, vol. 3, pp. 263–286, 2000.

[37] K. Yi and C. Faloutsos, "Fast time sequence indexing for arbitrary Lp norms," in *Proc. 26th Int. Conf. Very Large Databases*, Cairo, Egypt, 2000, pp. 385–394.

[38] E. Keogh, *The SAX Homepage* [Online]. Available: http://www.cs.ucr.edu/~eamonn/SAX.htm, 2015

[39] J. Lin, E. Keogh, L. Wei, and S. Lonardi, "Experiencing SAX: A novel symbolic representation of time series," *Data Mining Knowl. Discovery*, vol. 15, no. 2, pp. 107–144, 2007.

[40] G. Georgoulas, P. Karvelis, T. Loutas, and C. D. Stylios, "Rolling element bearings diagnostics using the symbolic aggregate approximation," *Mech. Syst. Signal Process.*, vol. 60, pp. 229–242, 2015.

[41] V. Rajagopalan and A. Ray, "Wavelet-based space partitioning for symbolic time series analysis," in *Proc. 44th IEEE Conf. Decision Control Eur. Control Conf. (CDC-ECC'05)*, 2005, pp. 5245–5250.

[42] V. Rajagopalan and A. Ray, "Symbolic time series analysis via wavelet-based partitioning," *Signal Process.*, vol. 86, no. 11, pp. 3309–3320, 2006.

[43] N. Kumar, V. N. Lolla, E. J. Keogh, S. Lonardi, and C. Ratanamahatana, "Time-series Bitmaps: A practical visualization tool for working with large time series databases," in *Proc. 5th SIAM Int. Conf. Data Mining SDM*, 2005, pp. 531–535.

[44] J. Lin, R. Khade, and Y. Li, "Rotation-invariant similarity in time series using bag-of-patterns representation," *J. Intell. Inf. Syst.*, vol. 39, no. 2, pp. 287–315, 2012.

[45] H. J. Koskimaki, P. Laurinen, E. Haapalainen, L. Tuovinen, and J. Roning, "Application of the extended k nn method to resistance spot welding process identification and the benefits of process information," *IEEE Trans. Ind. Electron.*, vol. 54, no. 5, pp. 2823–2830, Oct. 2007.
[46] X. Jin, M. Zhao, T. W. Chow, and M. Pecht, "Motor bearing fault diagnosis using trace ratio linear discriminant analysis," *IEEE Trans. Ind. Electron.*, vol. 61, no. 5, pp. 2441–2451, May 2014.
[47] P. Domingos, "A few useful things to know about machine learning," *Commun. ACM*, vol. 55, no. 10, pp. 78–87, 2012.
[48] M. Pineda-Sanchez, V. Climente-Alarcon, M. Riera-Guasp, R. Puche-Panadero, and J. Pons-Llinares, "Enhanced simulink induction motor model for education and maintenance training," *System. Cybern. Inf.*, vol. 10, no. 2, pp. 92–97, 2012.
[49] N. Japkowicz and M. Shah, *Evaluating Learning Algorithms: A Classification Perspective*. Cambridge, U.K.: Cambridge Univ. Press, 2011.

Petros Karvelis received the B.Sc., M.Sc., and Ph.D. degrees in computer science from the University of Ioannina, Ioannina, Greece, in 2001, 2004, and 2012, respectively.

He is currently a Postdoctorate Research Fellow with the Knowledge and Intelligent Computing Laboratory, Department of Computer Engineering, Technological Educational Institute of Epirus, Arta, Greece. His research interests include machine learning, image processing, biomedical engineering, and decision-support systems.

George Georgoulas received the Dipl.-Eng. and Dr.-Eng. degrees in electrical and computer engineering from the University of Patras, Patras, Greece, in 1999 and 2006, respectively.

He is currently a Postdoctorate Research Fellow with the Knowledge and Intelligent Computing Laboratory, Department of Computer Engineering, Technological Educational Institute of Epirus, Arta, Greece. His research interests include machine learning, signal processing, failure detection, diagnosis, and decision-support systems.

Ioannis P. Tsoumas (S'04–M'08) was born in Athens, Greece. He received the Dipl.-Eng. and Dr.-Eng. degrees in electrical and computer engineering from the University of Patras, Patras, Greece, in 2000 and 2007, respectively.

From 2008 to 2015, he has been with Siemens AG, Industry Sector, Drive Technologies Division, Large Drives, Nuremberg, Germany. In 2015, he joined the ABB Corporate Research Center, Dättwil, Switzerland. His research interests include electrical machines and drives condition monitoring and fault diagnosis, modulation techniques for power converters, converters and drive systems efficiency, as well as motor-converter interaction.

Dr. Tsoumas is Member of the Association for Electrical, Electronic, and Information Technologies (VDE) and the Technical Chamber of Greece.

Jose Alfonso Antonino-Daviu (S'04–M'08–SM'12) received the M.S. and Ph.D. degrees in electrical engineering from the Universitat Politecnica de Valencia, Valencia, Spain, in 2000 and 2006, respectively.

Currently, he is an Associate Professor with the Department of Electrical Engineering, Universitat Politecnica de Valencia, where he develops his docent and research work. He has been an Invited Professor with the Helsinki University of Technology, Otaniemi, Finland, in 2005 and 2007; Michigan State University, East Lansing, MI, USA, in 2010; Korea University, Seoul, Korea, in 2014; and Universite Claude Bernard Lyon 1, Villeurbanne, France, in 2015. He has authored over 100 papers in international journals, conferences, and books. His research interests include condition monitoring of electric machines, wavelet theory and its application to fault diagnosis and design, and optimization of electrical installations and systems.

Vicente Climente-Alarcón (S'11–M'12) received the M.Sc. degree in chemical and industrial engineering, and the Ph.D. degree in electrical engineering from the Universitat Politecnica de Valencia, Valencia, Spain, in 2000, 2011, and 2012.

He has worked as an Assistant Professor with the School of Industrial Engineering, Universitat Politecnica de Valencia, on research tasks in the area of condition monitoring of electrical machines, and externally as a Consultant in automation and management of power systems. Currently, he is a Postdoctoral Research Fellow with the Department of Electrical Engineering and Automation, Aalto University, Espoo, Finland. His research interests include the study of transients in electrical machines.

Chrysostomos D. Stylios (M'97–SM'15) received the Diploma degree in electrical and computer engineering from the Aristotle University of Thessaloniki, Thessaloniki, Patras, Greece, in 1992, and the Ph.D. degree in electrical and computer engineering from the University of Patras, Patras, Greece, in 1999.

He is an Associate Professor with the Department of Computer Engineering, Technological Educational Institute of Epirus, Arta, Greece. He was a Visiting Researcher with the Department of Electrical and Computer Engineering, University of Alberta, Edmonton, AB, Canada, and the Department of Computer Science, University of Texas at El Paso, El Paso, TX, USA, for the academic year 2014–2015. He has authored over 160 journal and conference papers and book chapters. His research interests include fuzzy cognitive maps, soft computing, computational intelligence techniques, signal processing methods, and decision support systems.

Dr. Stylios is a Member of the TC 8.2 and TC 5.4 of International Federation of Automatic Control.